

TIME-VARYING AEROELASTIC MODELING AND FLUTTER ANALYSIS OF TELESCOPIC WINGS

Chun-Yan Li[1,2], Shun He[1,2], Zhi-Chun Yang[1,2,*]

[1]School of Aeronautics, Northwestern Polytechnical University, Xi'an, 710072, PR China
[2]National Key Laboratory of Strength and Structural Integrity, Xi'an, 710072, PR China

Abstract

Telescopic wings can meet different mission requirements by changing the wingspan. This paper investigates the time-varying aeroelastic characteristics of telescopic wings. A two-stage telescopic wing is simplified into an axially moving stepped beam. The structural model particularly considering the overlapping region of the telescopic wing is established based on Euler-Bernoulli beam theory and extended Hamilton's principle. The time-domain unsteady aerodynamic forces are estimated using a Padé approximation of Theodorsen's function. Then the time-varying aeroelastic state-space model is derived. The effects of wingspan, overlapping region, and morphing rate on the flutter boundaries and transient aeroelastic responses are studied. The results show that wingspan and overlapping region have significant influences on the aeroelastic behavior, and increasing the morphing rate reduces the peak amplitude of the aeroelastic response during the morphing process.

Keywords: Morphing aircraft, Telescopic wing, Time-varying aeroelasticity, Flutter, Stepped beam

1. Introduction

Morphing aircraft can adjust their geometric configuration during flight to achieve optimal performance and represent one of the most promising research directions in the aviation field. The telescopic wing is a typical and effective concept for morphing aircraft, which can change the aircraft's wingspan to adapt to different flight conditions [1]. However, the properties of the telescopic wing, such as mass distribution, damping characteristics, and aerodynamic characteristics, change over time [2], which leads to significant time-varying aeroelastic problems. Therefore, it is crucial to establish a time-varying aeroelastic model for the telescopic wing and to analyze its dynamic characteristics during the morphing process.

In previous studies, researchers usually simplified telescopic wings to axially moving uniform beams or plates to conduct aeroelastic analyses [3-5]. In practice, a telescopic wing generally contains several parts, including a fixed wing and multiple moving wings, and its structural characteristics more closely resemble an axially moving stepped beam. However, there are few studies on the time-varying aeroelasticity of multi-stage telescopic wings. Huang et al. [6] built a first-order state-space aeroelastic model for a telescopic wing consisting of an inboard wing and a movable outboard wing and calculated its flutter boundaries under different quasi-static configurations. Ajaj et al. [7] developed an aeroelastic model of a three-segment stepped telescopic wing, investigated the effects of each segment's structural parameters on aeroelastic behavior, and assessed the viability of span morphing for flutter suppression. Barzani et al. [8] constructed an aeroelastic model of a two-stage telescopic wing where the overlapping region was simulated as a time-varying lumped mass at the tip of the fixed part, and then analyzed how lumped mass, span length, and morphing speed affected the flutter stability.

Overall, the time-varying aeroelasticity of multi-stage telescopic wings has not been extensively studied, particularly regarding the effects of overlapping regions between adjacent stages. This work aims to investigate the time-varying aeroelastic behavior of telescopic wings. A two-stage telescopic wing is modeled as an axially moving cantilever stepped beam. An explicitly time-dependent

aeroelastic state-space model considering the overlapping region between the fixed wing stage and the moving wing stage is developed. The proposed method can be extended to multi-stage telescopic wings, providing a general framework for the theoretical modeling of such configurations. The effects of wingspan, overlapping region, and morphing rate on the flutter stability and transient aeroelastic responses are illustrated.

2. Aeroelasticity Model

A schematic of the two-stage telescopic wing is shown in Figure 1. The blue outline represents the fixed wing stage, the red outline represents the moving wing stage, and the gray shaded area indicates the overlapping region between the two stages. The moving wing stage can extend or retract axially relative to the fixed wing stage at a velocity of v_T. The length of the fixed wing stage and the total wingspan are denoted by L_f and $L(t)$, respectively.

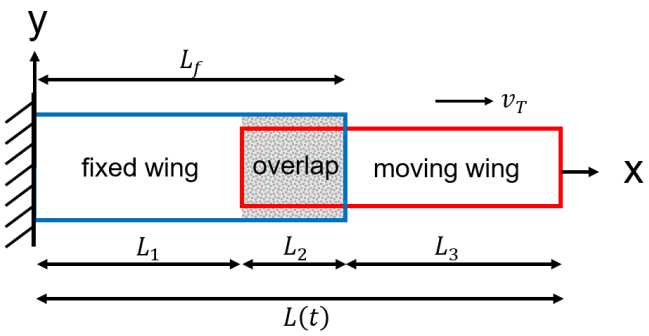


Figure 1 – Two-stage telescopic wing

The two-stage telescopic wing is simplified to a stepped Euler-Bernoulli beam composed of three segments, corresponding to the fixed region, the overlapping region, and the outboard region. The lengths of the fixed region and the outboard region are L_1 and L_3, respectively. The overlapping region has a length of L_2 and contains both a portion of the fixed wing stage and a portion of the moving wing stage.

Considering bending (h_i) and torsional (θ_i) degrees of freedom of each segment, the governing equations of motion are derived based on extended Hamilton's principle as follows:

$$\begin{cases} m_i \dfrac{d^2 h_i}{dt^2} - m_i x_{\theta i} \dfrac{d^2 \theta_i}{dt^2} + EI_i \dfrac{d^4 h_i}{dx^4} = L_i' \\ -m_i x_{\theta i} \dfrac{d^2 h_i}{dt^2} + m_i r_{\theta i}^2 \dfrac{d^2 \theta_i}{dt^2} - GJ_i \dfrac{d^2 \theta_i}{dx^2} = M_{eai}' \end{cases}, i = 1,2,3 \tag{1}$$

where m_i is the mass per unit span, $x_{\theta i}$ is the distance between the elastic axis and the center of gravity, $r_{\theta i}$ is the radius of gyration about the elastic axis, EI_i is the bending rigidity, GJ_i is the torsional rigidity, L_i' is the lift per unit span, and M_{eai}' is the aerodynamic moment per unit span.

The structural parameters of the overlapping region ($i = 2$) are the sum of the corresponding parameters of the fixed and outboard regions [6], i.e., $m_2 = m_1 + m_3$, $EI_2 = EI_1 + EI_3$, $GJ_2 = GJ_1 + GJ_3$. Accordingly, the governing equations of motion for the overlapping region can be rewritten as:

$$\begin{cases} (m_1 + m_3) \dfrac{d^2 h_2}{dt^2} - (m_1 + m_3) x_{\theta 2} \dfrac{d^2 \theta_2}{dt^2} + (EI_1 + EI_3) \dfrac{d^4 h_2}{dx^4} = L_2' \\ -(m_1 + m_3) x_{\theta 2} \dfrac{d^2 h_2}{dt^2} + (m_1 + m_3) r_{\theta 2}^2 \dfrac{d^2 \theta_2}{dt^2} - (GJ_1 + GJ_3) \dfrac{d^2 \theta_2}{dx^2} = M_{ea2}' \end{cases} \tag{2}$$

It should be noted that only the moving wing stage is capable of axial motion. To better capture the physical behavior, the overlapping region is separated into fixed and moving parts. Different time derivative expressions (see Eq. (3) and Eq. (4)) and different modal superposition forms (see Eq. (8) and Eq. (9)) will be applied to each part.

For the fixed wing stage, the plunge and pitch displacements are functions of space, and the time derivatives are expressed as:

$$\begin{cases} \dfrac{dh_i}{dt} = \dfrac{\partial h_i}{\partial t} \\ \dfrac{d\theta_i}{dt} = \dfrac{\partial \theta_i}{\partial t} \\ \dfrac{d^2h_i}{dt^2} = \dfrac{\partial^2 h_i}{\partial t^2} \\ \dfrac{d^2\theta_i}{dt^2} = \dfrac{\partial^2 \theta_i}{\partial t^2} \end{cases} \tag{3}$$

For the moving wing stage, the plunge and pitch displacements depend on both space and time, so the time derivatives become:

$$\begin{cases} \dfrac{dh_i}{dt} = v_T \dfrac{\partial h_i}{\partial x} + \dfrac{\partial h_i}{\partial t} \\ \dfrac{d\theta_i}{dt} = v_T \dfrac{\partial \theta_i}{\partial x} + \dfrac{\partial \theta_i}{\partial t} \\ \dfrac{d^2h_i}{dt^2} = \dfrac{\partial^2 h_i}{\partial t^2} + 2v_T \dfrac{\partial^2 h_i}{\partial x \partial t} + v_T^2 \dfrac{\partial^2 h_i}{\partial x^2} + \dot{v}_T \dfrac{\partial h_i}{\partial x} \\ \dfrac{d^2\theta_i}{dt^2} = \dfrac{\partial^2 \theta_i}{\partial t^2} + 2v_T \dfrac{\partial^2 \theta_i}{\partial x \partial t} + v_T^2 \dfrac{\partial^2 \theta_i}{\partial x^2} + \dot{v}_T \dfrac{\partial \theta_i}{\partial x} \end{cases} \tag{4}$$

Substituting Eq. (3) and Eq. (4) into Eq. (1) and Eq. (2) yields the vibration equations in partial differential form. To obtain the corresponding time-dependent ordinary differential equations, the instantaneous mode shape functions of the stepped beam are adopted as trial functions, and the vibration equations are discretized using the modified Galerkin method.

The bending and torsional mode shape functions for each segment can be expressed as:

$$\psi_i(x) = A_i \sin\left(\beta_i\left(x - x_{i-1}\right)\right) + B_i \cos\left(\beta_i\left(x - x_{i-1}\right)\right) + C_i \sinh\left(\beta_i\left(x - x_{i-1}\right)\right) + D_i \cosh\left(\beta_i\left(x - x_{i-1}\right)\right) \tag{5}$$

$$\phi_i(x) = E_i \sin\left(k_i\left(x - x_{i-1}\right)\right) + F_i \cos\left(k_i\left(x - x_{i-1}\right)\right) \tag{6}$$

β_i and k_i are defined as:

$$\beta_i = \left(\frac{m_i}{EI_i}\omega_h^2\right)^{1/4}, k_i = \left(\frac{m_i r_{\theta i}^2}{GJ_i}\omega_\theta^2\right)^{1/2} \tag{7}$$

where $i = 1,2,3$, A_i, B_i, C_i, D_i, E_i, and F_i are undetermined coefficients, $x_0 = 0$, $x_1 = L_1$, and $x_2 = L_f$. It should be noted that ω_h and ω_θ denote the bending and torsional natural frequencies of the entire telescopic wing, rather than those of an individual segment. These undetermined coefficients can be determined from the boundary conditions and continuity conditions, as detailed in Ref. [9].

For the fixed wing stage, the plunge and pitch displacements are expressed as a superposition of the above mode shape functions:

$$\begin{cases} h_i(x,t) = \sum_{j=1}^{n} \psi_{ij}(x) q_{hj}(t) = \boldsymbol{\psi}_i^T(x) \boldsymbol{q}_h(t) \\ \theta_i(x,t) = \sum_{j=1}^{n} \phi_{ij}(x) q_{\theta j}(t) = \boldsymbol{\phi}_i^T(x) \boldsymbol{q}_\theta(t) \end{cases} \tag{8}$$

For the moving wing stage, since the coordinate x varies with time, a new parameter $\xi = x / \left(L_f + L_3(t)\right)$ is introduced, which satisfies $L_1 / \left(L_f + L_3(t)\right) \le \xi \le 1$. By replacing x with ξ in the mode shape functions, the displacements can be expressed as:

$$\begin{cases} h_i(x,t) = \sum_{j=1}^{n} \psi_{ij}(\xi) q_{hj}(t) = \boldsymbol{\psi}_i^T(\xi) \boldsymbol{q}_h(t) \\ \theta_i(x,t) = \sum_{j=1}^{n} \phi_{ij}(\xi) q_{\theta j}(t) = \boldsymbol{\phi}_i^T(\xi) \boldsymbol{q}_\theta(t) \end{cases} \tag{9}$$

Substituting Eq. (8) and Eq. (9) into the partial differential vibration equations and integrating yields the discretized structural dynamic equations of the two-stage telescopic wing. The above modeling

approach can be readily generalized to multi-stage telescopic wings.

According to Theodorsen's unsteady aerodynamic theory, the lift and moment of each segment are expressed as:

$$L_i' = \pi\rho_a \frac{c_i^2}{4}\left(-\frac{d^2h_i}{dt^2} + V\frac{d\theta_i}{dt} - \frac{\hat{a}_i c_i}{2}\frac{d^2\theta_i}{dt^2}\right) + 2\pi\rho_a V \frac{c_i}{2} C(k)\left(-\frac{dh_i}{dt} + V\theta_i + \frac{c_i}{2}\left(\frac{1}{2} - \hat{a}_i\right)\frac{d\theta_i}{dt}\right) \tag{10}$$

$$M_{eai}' = L_i'\left(\frac{c_i}{4} + \frac{\hat{a}_i c_i}{2}\right) + \pi\rho_a \frac{c_i^3}{8}\left(\frac{1}{2}\frac{d^2h_i}{dt^2} - V\frac{d\theta_i}{dt} - \frac{c_i}{2}\left(\frac{1}{8} - \frac{\hat{a}_i}{2}\right)\frac{d^2\theta_i}{dt^2}\right) \tag{11}$$

where ρ_a is the air density, c_i is the chord length of each segment, V is the flight speed, $\hat{a}_i = 2x_{\theta i}/c_i - 1$, and $C(k)$ is Theodorsen's function. To obtain time-domain aerodynamic forces, this paper employs the Padé approximation given in Ref. [4]. $C(k)$ is first transformed into the Laplace domain, then expressed in state-space form. Finally, the time-domain aerodynamic model is derived. By coupling the structural dynamic model with the aerodynamic model, the discretized time-varying aeroelastic governing equations are obtained in the following compact form:

$$\boldsymbol{M}(t)\ddot{\boldsymbol{q}}(t) + \boldsymbol{C}(t)\dot{\boldsymbol{q}}(t) + \boldsymbol{K}(t)\boldsymbol{q}(t) = \boldsymbol{F}(t) \tag{12}$$

where $\boldsymbol{M}(t)$, $\boldsymbol{C}(t)$, $\boldsymbol{K}(t)$ are the mass, damping, and stiffness matrices, respectively.

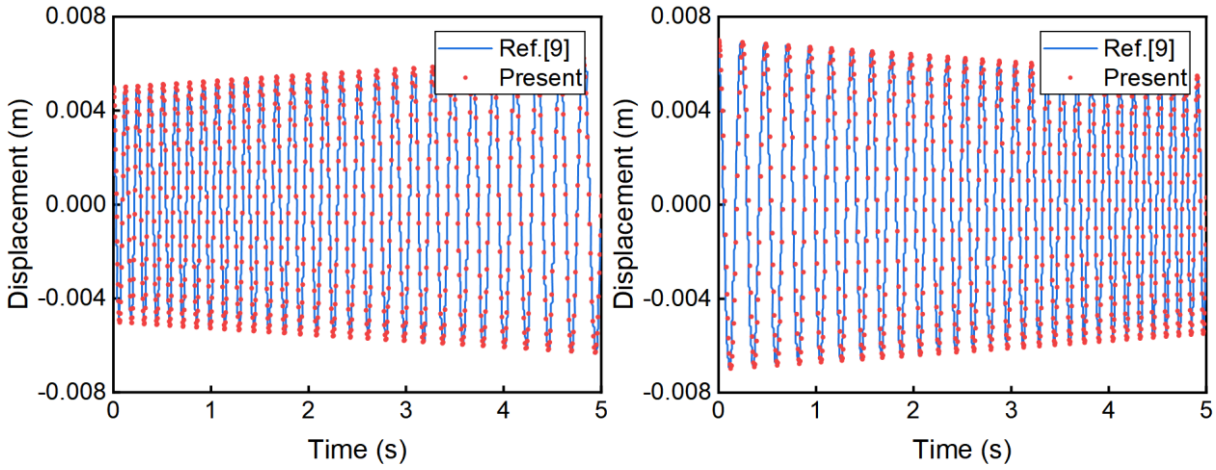
Eq. (12) can be rewritten in the following state-space form:

$$\dot{\boldsymbol{x}}(t) = \boldsymbol{A}(t)\boldsymbol{x}(t) \tag{13}$$

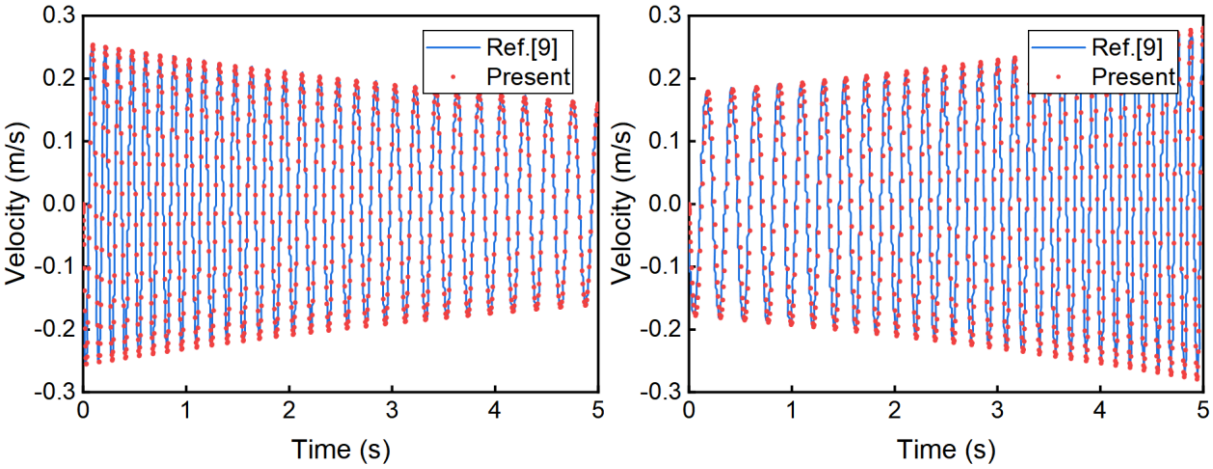
3. Verification

The proposed theoretical model is validated in two aspects: the structural dynamic model and the aeroelastic model. First, the transverse displacement and velocity responses of a stepped beam during axial extension are calculated. The structural parameters of the stepped beam are taken from Ref. [9]. As shown in Figure 2, the present results are in excellent agreement with the literature.

Then, the aeroelastic model is validated using two fixed wing models, i.e., HALE wing [10] and Goland wing [11], whose parameters are listed in Table 1. A comparison between the present results and those in Ref. [7] is shown in Table 2. The results indicate that retaining the first bending and first torsional modes is sufficient to accurately predict the flutter speed and flutter frequency.



(a) Displacement response ($v_T = 0.1$ m/s) (b) Displacement response ($v_T = -0.1$ m/s)



(c) Velocity response ($v_T = 0.1\ \mathrm{m/s}$) (d) Velocity response ($v_T = -0.1\ \mathrm{m/s}$)

Figure 2 – Validation of the structural dynamic model

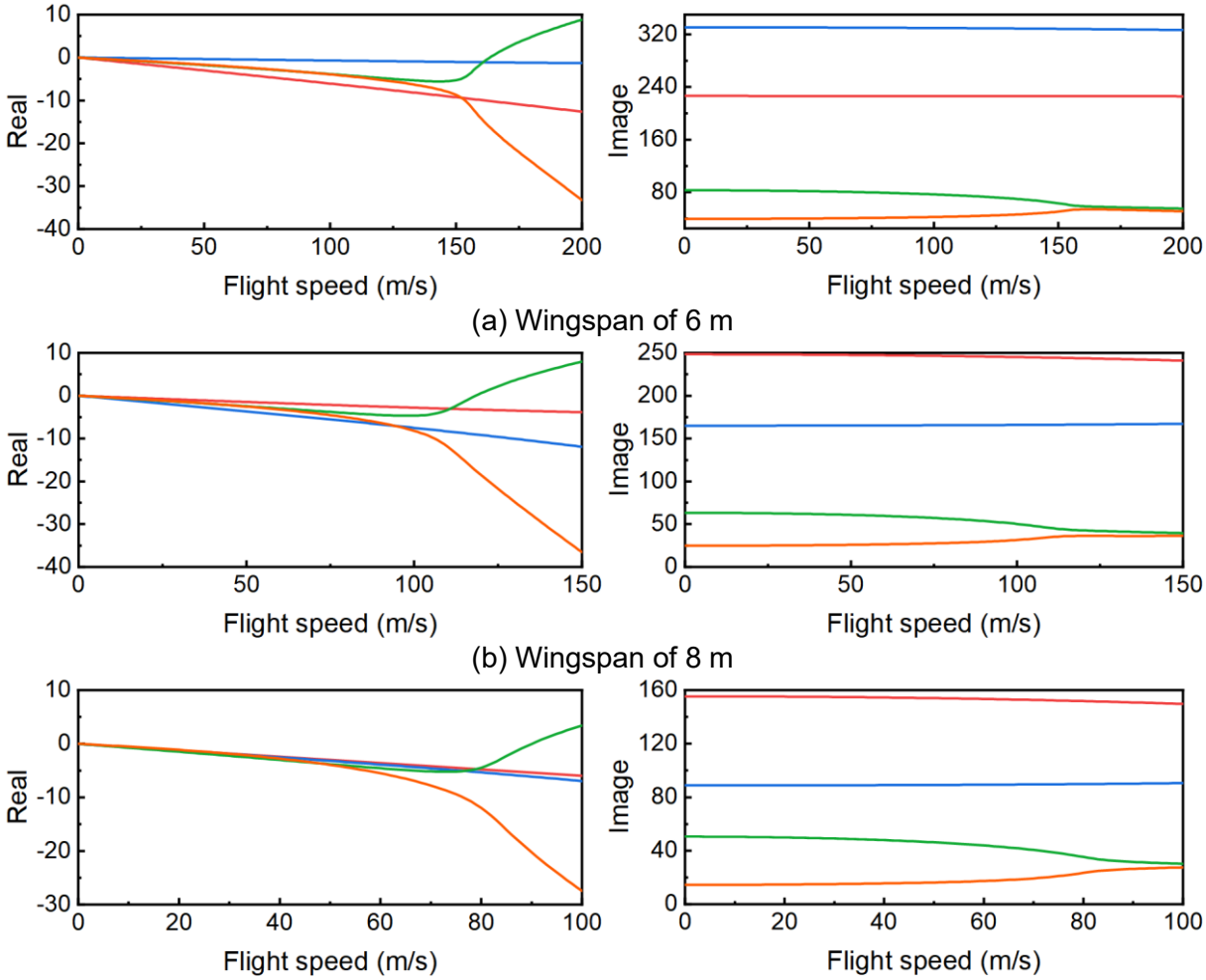
Table 1 – Parameters of the HALE wing and Goland wing

Parameter	HALE wing	Goland wing
Span (m)	16	6.096
Chord (m)	1	1.8288
Mass per unit span (kg/m)	0.75	35.71
Moment of inertia (kg·m)	0.1	8.64
Spanwise elastic axis	50% of chord	33% of chord
Gravity center	50% of chord	43% of chord
Bending rigidity ($N \cdot m^2$)	2×10^4	9.77×10^6
Torsional rigidity ($N \cdot m^2$)	1×10^4	9.87×10^5
Air density (kg/m^3)	0.0889	1.225

Table 2 – Comparison of aeroelastic test models

		Present (2 modes)	Ref.[7]	Difference
HALE Wing	Flutter speed (m/s)	33.43	33.00	1.30%
	Flutter frequency (rad/s)	21.39	21.75	1.66%
Goland Wing	Flutter speed (m/s)	136.81	137.01	0.15%
	Flutter frequency (rad/s)	69.83	69.93	0.14%

The aeroelastic behavior of a two-stage telescopic wing will be investigated. In this study, the telescopic wing comprises a fixed wing stage and a moving wing stage, with the Goland wing's cross-sectional properties. The fixed and moving wing stages have lengths of 6 m and 5 m, respectively. The total wingspan can extend from 6 m (fully retracted) to 11 m (fully extended). The trajectories of the center of gravity and the shear center of the telescopic wing are assumed to be two straight lines. Figure 3 shows the variation of the flutter modes at different wingspans when the first two bending modes and first two torsional modes are retained. It is evident that, throughout the entire wingspan range, the first bending mode and the first torsional mode are the dominant flutter modes. Therefore, for simplicity, only two modes (1st bending, 1st torsion) are retained for the following time-varying aeroelastic analysis.



(a) Wingspan of 6 m

(b) Wingspan of 8 m

(c) Wingspan of 11 m

Figure 3 – Flutter modes at different wingspans (orange for 1st bending, green for 1st torsion, blue for 2nd bending, red for 2nd torsion)

4. Results and discussion

The effects of the overlapping region, wingspan and morphing rate on the aeroelastic behavior will be studied in this section. To examine the influence of the overlapping region on the aeroelastic characteristics of the telescopic wing, two cases are defined:

Case 1. Considering the moving part of the overlapping region.

Case 2. Neglecting the moving part of the overlapping region.

It should be noted that, in Case 2, the telescopic wing can be simplified to a two-segment stepped beam, including the fixed segment and the outboard segment, whereas in Case 1, it has to be modeled as a three-segment stepped beam.

4.1 Variation of natural frequencies and mode shapes

Figure 4 presents the first two natural frequencies of the telescopic wing at different varying wingspan for Case 1 and Case 2. As the wingspan increases, the natural frequencies gradually decrease with a descending rate. Comparing the two cases, it can be seen that neglecting the moving part of the overlapping region results in higher natural frequencies for both bending and torsional modes, since the reduction in total mass exceeds the reduction in total stiffness. Moreover, as the moving wing stage extends, the overlapping region shrinks, so the difference in natural frequencies between the two cases narrows.

Figure 5 illustrates the mode shapes at wingspans of 8 m and 10 m. It is evident that neglecting the moving part of the overlapping region leads to significant distortions in the mode shapes, especially the torsional mode shape, and the larger the overlapping region, the more severe the distortion. This indicates that the overlapping region plays an important role on the modal characteristics of the telescopic wing.

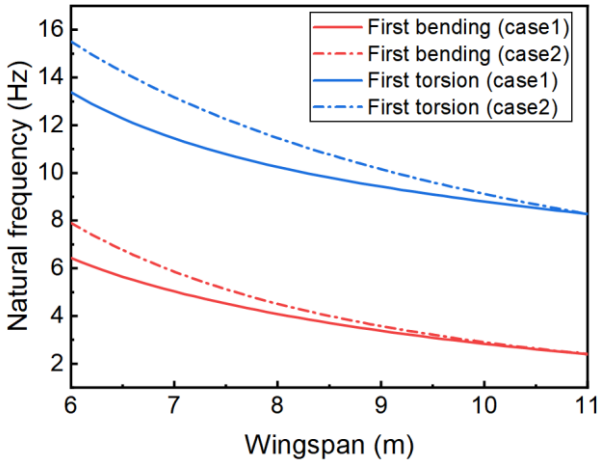
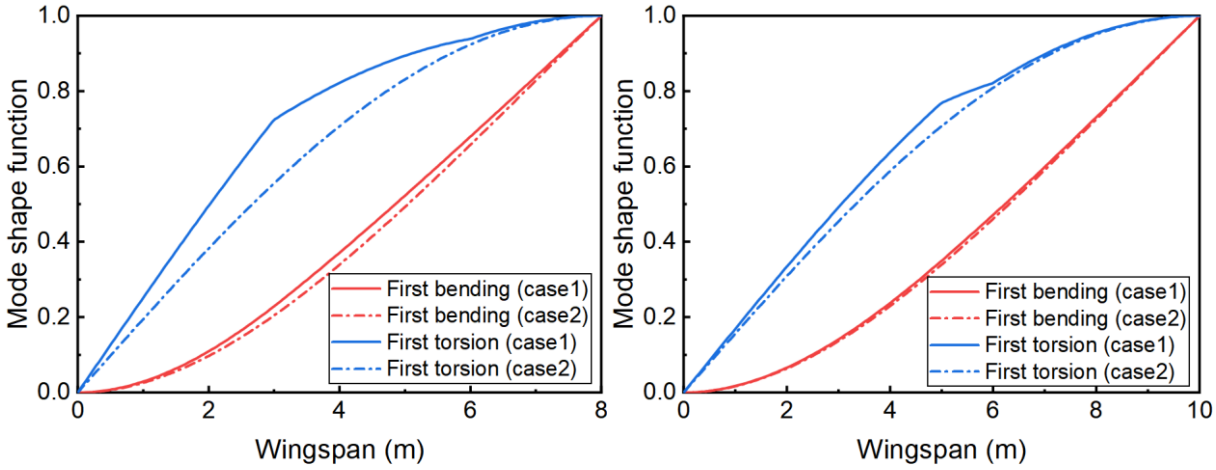


Figure 4 – Variation of natural frequencies with wingspan



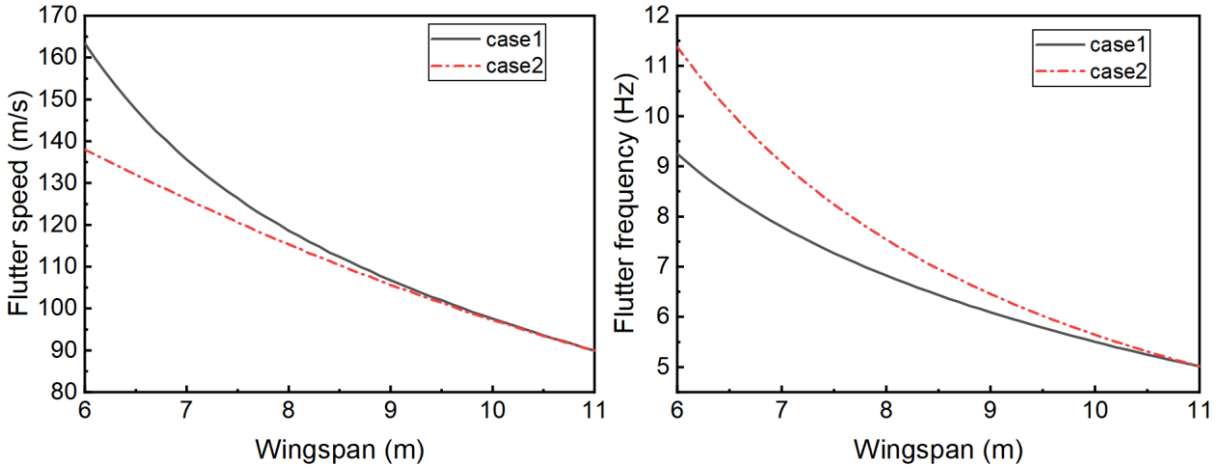
(a) Wingspan of 8 m (b) Wingspan of 10 m

Figure 5 – Mode shape comparison

4.2 Variation of flutter characteristics

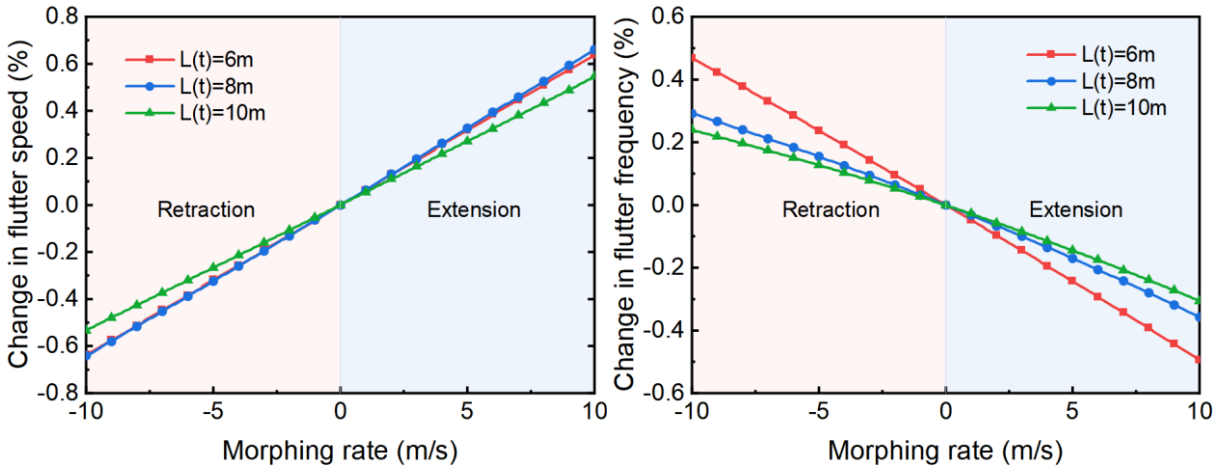
To investigate the effects of wingspan and overlapping region on the flutter boundary, the flutter speed and flutter frequency are calculated for Case 1 and Case 2 under quasi-static wingspan variation (zero morphing rate). As shown in Figure 6, when the telescopic wing extends from the fully retracted configuration to the fully extended configuration, both the flutter speed and flutter frequency decrease significantly with a decreasing rate. This is due to the reduction in the wing's natural frequencies with increasing wingspan. Comparison of Case 1 and Case 2 reveals that neglecting the moving part of the overlapping region lowers the flutter speed but raises the flutter frequency. At full retraction (largest overlap), such neglect reduces the flutter speed by 15.54% and increases the flutter frequency by 23.06%. The result indicates that the overlapping region significantly affects the calculation of flutter characteristics. As the overlapping region shrinks, the differences in flutter between the two cases gradually decrease.

The effect of morphing rate on the flutter boundary is then studied. The wingspan is fixed at three values: 6 m, 8 m, and 10 m. The morphing rate varies from -10 m/s (retraction) to 10 m/s (extension). The computed flutter speed and flutter frequency are shown in Figure 7. It should be noted that Figure 7 shows the percentage change relative to the quasi-static results for each configuration. The results show that during extension, increasing the morphing rate raises the flutter speed and lowers the flutter frequency, but during retraction, it lowers the flutter speed and raises the flutter frequency. Furthermore, Figure 7(a) shows that the flutter speed variation with morphing rate is insensitive to wingspan, while Figure 7(b) shows that the flutter frequency is more sensitive to morphing rate at smaller wingspans.



(a) Flutter speed (b) Flutter frequency

Figure 6 – Effects of wingspan and overlapping region on the flutter boundary



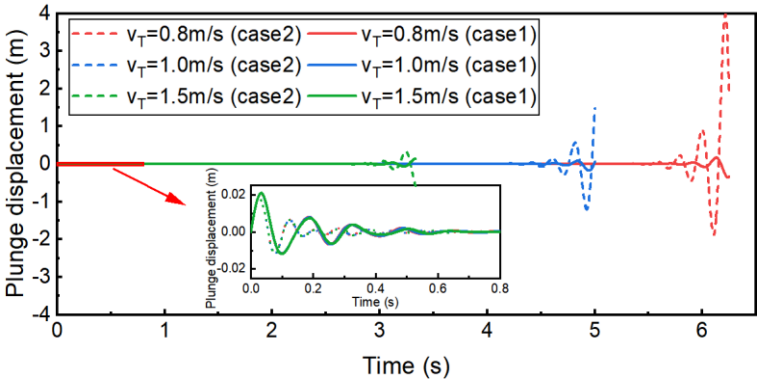
(a) Flutter speed (b) Flutter frequency

Figure 7 – Effect of morphing rate on the flutter boundary

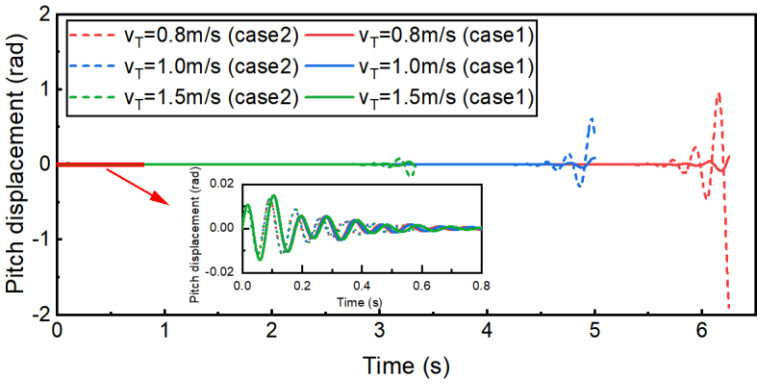
4.3 Transient aeroelastic response

This section evaluates the effects of morphing rate and overlapping region on the transient aeroelastic response of the telescopic wing. Figure 8 presents the wingtip plunge and pitch displacements during uniform extension of the wingspan from 6 m to 11 m at a flight speed of 114 m/s. Figure 9 presents the wingtip plunge and pitch displacements during uniform retraction from 11 m to 6 m at a flight speed of 110 m/s. The initial conditions are set as $\dot{h}=1\ \mathrm{m/s}$ and $\dot{\theta}=1\ \mathrm{rad/s}$. The morphing rates are taken as 0.8 m/s, 1.0 m/s, and 1.5 m/s. For comparison, the results of Case 2 are also included.

As shown in Figure 8, during wingspan extension, the plunge and pitch displacements initially converge and then diverge, and increasing the extension rate reduces the maximum displacement or the peak amplitude. Meanwhile, the response amplitude is significantly larger in Case 2 relative to Case 1 at the same extension rate. It can be seen from Figure 9 that, during retraction, the displacement responses first diverge and then converge, and the peak amplitude decreases with higher retracting rates. The response amplitude in Case 2 is slightly larger than that in Case 1 at the same retraction rate. Overall, increasing the morphing rate helps suppress the peak amplitude of the transient aeroelastic responses during both extension and retraction, thus enhancing dynamic stability during the morphing process. The overlapping region affects the aeroelastic response throughout the morphing process, particularly during extension. Therefore, it should be accounted for in the modeling.

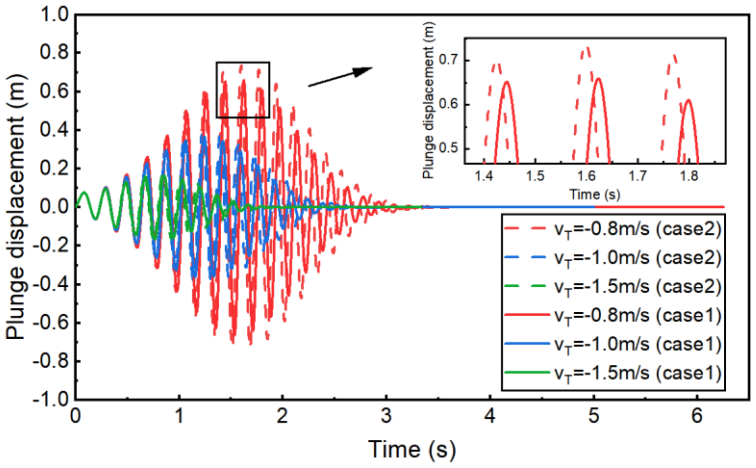


(a) Plunge displacement

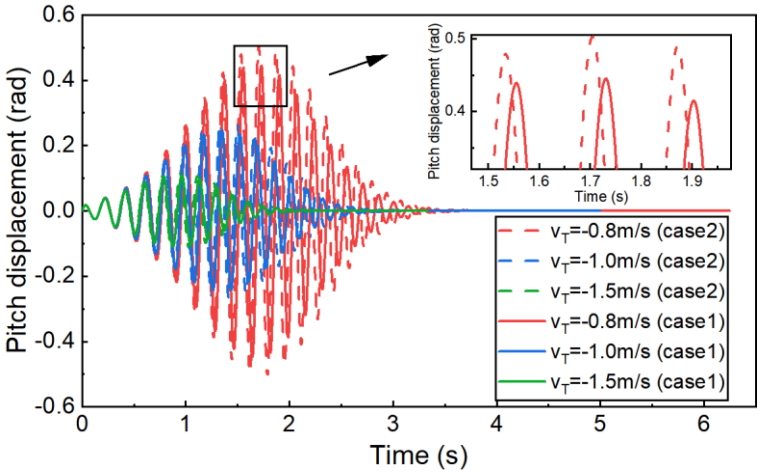


(b) Pitch displacement

Figure 8 – Aeroelastic responses during extension



(a) Plunge displacement



(b) Pitch displacement

Figure 9 – Aeroelastic responses during retraction

5. Conclusions

In this paper, a time-varying aeroelastic state-space model for a two-stage telescopic wing has been developed. The wing is modeled as a stepped Euler-Bernoulli beam composed of three segments. Euler-Bernoulli beam theory and extended Hamilton's principle are used to establish the structural model. Theodorsen's unsteady aerodynamic theory is adopted to estimate the aerodynamic loads. The effects of wingspan, overlapping region, and morphing rate on the aeroelastic behavior of the telescopic wing are systematically investigated. The conclusions are drawn as follows:

(1) As the wingspan increases, the natural frequencies, flutter speed, and flutter frequency of the telescopic wing decrease.

(2) The overlapping region has a significant influence on the modal characteristics, flutter characteristics, and transient aeroelastic response.

(3) During extension, increasing the morphing rate raises the flutter speed and reduces the flutter frequency, while the opposite trends are observed during retraction.

(4) A faster morphing rate helps reduce the peak amplitude of aeroelastic response and enhance dynamic stability during the morphing process.

6. Acknowledgment

The authors acknowledge the financial support by National Natural Science Foundation of China (Grant No. 12372170 and 12102317).

7. Contact Author Email Address

E-mail: yangzc@nwpu.edu.cn

8. Copyright Statement

The authors confirm that they, and/or their company or organization, hold copyright on all of the original material included in this paper. The authors also confirm that they have obtained permission, from the copyright holder of any third party material included in this paper, to publish it as part of their paper. The authors confirm that they give permission, or have obtained permission from the copyright holder of this paper, for the publication and distribution of this paper as part of the ICAS proceedings or as individual off-prints from the proceedings.

References

[1] Ajaj RM, Parancheerivilakkathil MS, Amoozgar M, et al. Recent developments in the aeroelasticity of morphing aircraft. *Progress in Aerospace Sciences*, Vol. 120, pp 100682, 2021.

[2] Zhang W, Gao YH, Guo XT, et al. Nonlinear time-varying vibrations of axially moving nested composite cantilever wing under aerodynamic force. *Mechanical Systems and Signal Processing*, Vol. 224, pp 112118, 2025.

[3] Huang R and Qiu ZP. Transient aeroelastic responses and flutter analysis of a variable-span wing during the morphing process. *Chinese Journal of Aeronautics*, Vol. 26, No. 6, pp 1430-1438, 2013.

[4] Ajaj RM and Friswell MI. Aeroelasticity of compliant span morphing wings. *Smart Materials and Structures*, Vol. 27, No. 10, pp 105052, 2018.

[5] Li WC and Jin DP. Flutter suppression and stability analysis for a variable-span wing via morphing technology. *Journal of Sound and Vibration*, Vol. 412, pp 410-423, 2018.

[6] Huang R, Qiu ZP and Wang XJ. Continuum aeroelastic model and flutter analysis for a variable-span morphing wing. *Applied Mechanics and Materials*, Vols. 300-301, pp 1136-1143, 2013.

[7] Ajaj RM, Omar FK, Darabseh TT, et al. Flutter of telescopic span morphing wings. *International Journal of Structural Stability and Dynamics*, Vol. 19, No. 6, pp 1950061, 2019.

[8] Barzani SHM, Shahverdi H and Amoozgar M. Parametric study on the dynamic aeroelastic analysis of a two-stage axially deploying telescopic wing. *Journal of Vibration and Control*, Vol. 29, No. 9-10, pp 2021-2034, 2023.

[9] Duan Y-C, Wang J-P, Wang J-Q, et al. Theoretical and experimental study on the transverse vibration properties of an axially moving nested cantilever beam. *Journal of Sound and Vibration*, Vol. 333, No. 13, pp 2885-2897, 2014.

[10] Patil MJ, Hodges DH and Cesnik CES. Nonlinear aeroelasticity and flight dynamics of high-altitude long-endurance aircraft. *Journal of Aircraft*, Vol. 38, No. 1, pp 88-94, 2001.

[11] Goland M. The flutter of a uniform cantilever wing. *Journal of Applied Mechanics*, Vol. 12, No. 4, pp A197-A208, 1945.